Biomimetic asymmetric bacterial membranes incorporating lipopolysaccharides

Mareike S. Stephan,[1] Valentin Dunsing,[2,3] Shreya Pramanik,[1] Salvatore Chiantia,[3] Stefanie Barbirz,[4] Tom Robinson,[1,*] and Rumiana Dimova[1,*]

[1]Max Planck Institute of Colloids and Interfaces, Potsdam, Germany; [2]Aix-Marseille Université, CNRS, IBDM, Turing Center for Living Systems, Marseille, France; [3]University of Potsdam, Institute of Biochemistry and Biology, Potsdam, Germany; and [4]Department Humanmedizin, MSB Medical School Berlin, Berlin, Germany

ABSTRACT   Gram-negative bacteria are equipped with a cell wall that contains a complex matrix of lipids, proteins, and glycans, which form a rigid layer protecting bacteria from the environment. Major components of this outer membrane are the high-molecular weight and amphiphilic lipopolysaccharides (LPSs). They form the extracellular part of a heterobilayer with phospholipids. Understanding LPS properties within the outer membrane is therefore important to develop new antimicrobial strategies. Model systems, such as giant unilamellar vesicles (GUVs), provide a suitable platform for exploring membrane properties and interactions. However, LPS molecules contain large polysaccharide parts that confer high water solubility, which makes LPS incorporation in artificial membranes difficult; this hindrance is exacerbated for LPS with long polysaccharide chains, i.e., the smooth LPS. Here, a novel emulsification step of the inverted emulsion method is introduced to incorporate LPS in the outer or the inner leaflet of GUVs, exclusively. We developed an approach to determine the LPS content on individual GUVs and quantify membrane asymmetry. The asymmetric membranes with outer leaflet LPS show incorporations of 1–16 mol % smooth LPS (corresponding to 16–79 wt %), while vesicles with inner leaflet LPS reach coverages of 2–7 mol % smooth LPS (28–60 wt %). Diffusion coefficient measurements in the obtained GUVs showed that increasing LPS concentrations in the membranes resulted in decreased diffusivity.

SIGNIFICANCE   This research article introduces a new method to create artificial biomembranes that mimic the cell envelope of Gram-negative bacteria. The membrane system represents artificial cell mimetic, namely giant vesicles that incorporate the bacterial cell wall component lipopolysaccharide (LPS). LPSs are amphiphilic molecules that show challenging properties regarding membrane incorporation mainly because of their high self-aggregation rate and their polydisperse size. These amphiphiles are known to form a hydrophilic barrier and provide rigidity that hinders the entry of antimicrobial substances. In the context of the emerging spread of antibiotic resistances, this membrane model system can be employed to study the properties and relevance of LPS to develop new antimicrobial strategies.

INTRODUCTION

The Gram-negative outer membrane (OM) as the outermost structure of the bacterial cell envelope forms a barrier toward the extracellular space. In the context of the global challenge of antibiotic resistances (1), understanding the biophysical properties at the bacterial cell surface is critical. Lipopolysaccharides (LPS) are found in the exterior leaflet

of OM and provide a hydrophilic barrier that hinders the penetration of hydrophobic substances, macromolecules, and antimicrobial agents (2). LPS are amphiphilic molecules that are composed of the membrane anchor lipid A ($\sim$2.3 kDa), a core saccharide ($\sim$2.5 kDa) and a facultative polysaccharide chain, called the O-antigen (2.5–25 kDa). Lipid A consists of a phosphorylated diglucosamine group that fixes the molecules via four to seven acyl chains (generally C_{10}-C_{16} chains) in the membrane (2–4), and is covalently linked to the core saccharide (4,5). The outermost structure is the O-antigen, which can extend up to 10 nm from the bacterial surface (2,3). The length of the O-antigen for different LPS molecules varies according to metabolic state and environmental conditions (5), resulting

in polydisperse size distributions. LPS molecules equipped with the O-antigen are classified as smooth LPS, whereas truncated molecules lacking the polysaccharide moiety are referred to as rough LPS (4). In the OM, divalent cations bridge the negatively charged phosphate groups of LPS and contribute to a rigid and highly stable barrier. Removal of the cations reduces membrane stability and renders the cell envelope permeable (6).

The incorporation of LPS molecules in model membranes is challenging owing to the unique properties of LPS, and the difficulties are particularly exacerbated for the smooth LPS. The smooth LPS of *Salmonella enterica* subsp. *enterica* (*S.*) Typhimurium is water soluble but shows a high aggregation rate with a critical micelle concentration of about 10–20 μg mL^{-1} (7). The micellar state is very stable and it is assumed that, even below the critical micelle concentration, LPS is present rather as small self-assembled structures than as free molecules. This makes the release of LPS molecules for integration into artificial membranes or assembly at water-oil interfaces less favorable. Moreover, due to size polydispersity, the solubility of the different LPS molecules in aqueous solutions varies depending on the length of the O-antigen chain (7). This changes both the affinity for incorporation into membranes and the adsorption at water-oil interfaces.

Model membranes allow the study of effects and contributions of individual components by eliminating the biological complexity and thus interference of different cell envelope components. Giant unilamellar vesicles (GUVs) are versatile tools, as they represent cell-sized free-standing bilayers that can be observed with an optical microscope (8). GUVs opened up various lines of synthetic biology research toward building artificial cells with specialized functionality (9,10). A number of methods exist for the preparation of these systems (8,11–16). The most widely used approaches rely on dissolving the membrane components (e.g., lipids) in an organic solvent, depositing and drying this solution on a substrate, followed by subsequent swelling of the formed lipid bilayers in the presence of an aqueous solution, either spontaneously or under the influence of electric field or osmosis (these methods include the so-called spontaneous swelling, electroformation, and gel-assisted swelling (16)). These approaches are not easily amenable to introducing smooth LPS at a substantial fraction because the LPS molecules are not soluble in the organic solvents. Even if this difficulty is overcome, the membranes obtained with these methods would have symmetric leaflets. Kubiak et al. have succeeded in producing symmetric LPS-GUVs via the electroformation protocol (17) via a two-step process, including LPS incorporation in oligolamellar vesicles (employing a dehydration-rehydration approach as introduced earlier (18)) and further purification from free LPS. Smooth LPS molecules could be incorporated up to 14 mol %, while rough LPS could be incorporated up to 25 mol % (17). The obtained LPS-GUVs revealed different phase behaviors: while the presence of rough LPS mole-

cules resulted in the formation of micrometer-sized gel-like domains (17,19,20), GUVs containing smooth LPS appeared homogeneous under microscopy observations, but seemed to form submicroscopic clusters at higher concentration (17). Similarly, Nair et al. (21) formed LPS containing GUVs employing the gel-assisted swelling method (22). All of these approaches allowed the formation of GUVs with a symmetric LPS distribution at the inner and outer leaflet of the membrane. Since asymmetry is an important property of OM, synthesizing membranes with asymmetric LPS distribution would yield a more accurate model of real bacterial membrane.

The production of GUVs with asymmetric membrane leaflets became possible with the introduction of the phase-transfer method (also known as droplet-transfer or emulsion transfer), first pioneered by Träuble and Grell (23), and later commented on by Szoka and Papahadjopoulos (24), and popularized with the reports by Weitz and co-workers (25) as well as by Noireaux and Libchaber (26). These approaches rely on the stepwise assembly of the vesicle membrane leaflet by leaflet: first, preparing water droplets (suspended in a nonpolar solvent, i.e., oil) stabilized by one (mono)layer of lipids on their surface and, then, "enwrapping" the droplets by a second lipid layer to obtain the vesicle architecture. The process is aided by gravity, centrifugation, or microfluidic flow (see, e.g., (27)). Alternative approaches to generate GUVs with asymmetric membrane composition are based on hemifusion (28,29), cyclodextrin-mediated lipid exchange (30–32), and microfluidic jetting (33).

So far, only a few groups have managed the difficult task of preparing asymmetric LPS-GUVs. An approach was recently presented by Maktabi et al. using microfluidics to generate GUVs at high-throughput rates with asymmetric LPS distribution (34). Micropipette aspiration experiments showed that LPS molecules in the membrane cause a reduction in area expansion and bending modulus (34). The prepared vesicles had a monodisperse size distribution, which can be advantageous, due to the more homogeneous sample properties, facilitating comparison between different preparation conditions or for bulk studies. However, such microfluidic systems are very complex, difficult to handle, and not readily available in every laboratory. Thus, the alternative approach we considered for incorporating smooth LPS is the inverted emulsion technique, which allows the one-pot formation of symmetric and asymmetric GUVs aided not by microfluidics but by gravity or centrifugation (35,36). This approach requires only a simple benchtop centrifuge and sonication bath and is therefore applicable in most laboratory settings. Paulowski et al. demonstrated the applicability of this protocol by incorporation of rough (truncated) LPS mutants into asymmetric GUVs and verified the membrane asymmetry via a quenching assay (19). Rough LPS molecules can be treated similarly to lipids as they have similar solubility in chloroform and oil. The study demonstrated phase separation in membranes with rough LPS,

which supports the results of Kubiak et al. obtained with symmetric rough LPS GUVs (17). However, rough LPS molecules are only a small subset of the LPS variations found in the bacterial cell envelope. Since smooth LPS variants differ in their solubility properties and are not soluble in chloroform or oil, the protocol used requires adaptation for the integration of smooth LPS species.

In this work, we introduce a new inverted emulsion protocol for the incorporation of smooth LPS into asymmetric model membranes. We introduce modifications to the standard protocol for inverted emulsions to account for the properties of smooth LPS and improve the yield. In addition, we develop a technique for determining the LPS content on individual GUVs instead of bulk composition analysis. Moreover, we quantify membrane asymmetry and diffusion coefficients of LPS and lipids in the membrane.

MATERIALS AND METHODS

Chemicals and buffers

Polyvinyl alcohol (PVA), fully hydrolyzed, with a molecular weight of approximately 145 kDa, 6-carboxyfluorescein, and MgCl$_2$ were purchased from Merck (Darmstadt, Germany). Glucose, sucrose, chloroform, buffers (Tris and HEPES), NaCO$_3$, NaPO$_4$, NaIO$_4$, NaCl, sodium dithionite, MgSO$_4$, glycerol, DMSO, and β-casein (from bovine milk) were obtained from Sigma-Aldrich (St. Louis, Missouri, USA). Rhodamine B, Alexa647 hydrazide, and TexasRed hydrazide (also referred below as free TexasRed dye) were purchased from Thermo Fischer (Waltham, Massachusetts, USA). NBD hydrazine was purchased from Chemodex (St. Gallen, Switzerland). Light mineral oil was obtained in 10 mL glass bottles from Roth (Karlsruhe, Germany) and Sigma-Aldrich; larger bottle volumes were avoided to minimize effects of humidity.

Phospholipids

1-Palmitoyl-2-oleoyl-*sn*-glycero-3-phosphocholine (POPC) and 1,2-dioleoyl-*sn*-glycero-3-phosphoethanolamine-*N*-(7-nitro-2-1,3-benzoxadiazol-4-yl) (18:1 NBD-PE) were purchased from Avanti Lipids Polar, Alabaster, AL. TexasRed 1,2-dihexadecanoyl-*sn*-glycero-3-phosphoethanolamine was purchased from Thermo Fischer (Germany).

LPS isolation and labeling

The isolation of smooth LPS from *Salmonella enterica* subsp. *enterica* (*S.*) Typhimurium was achieved as described previously (37,38). To break up micellar structures and micelles, all LPS solutions were treated with five freeze/thaw cycles and 10 to 20 min sonication before usage.

LPS was labeled with either Alexa647 hydrazide, NBD hydrazine, or TexasRed hydrazide, employing the protocol from Kubiak et al. (17). In brief, 3 mg mL^{-1} LPS were dissolved in 900 μL 100 mM NaCO$_3$ (pH 5), mixed with 100 μL freshly prepared and ice-cold 100 mM NaIO$_4$ and incubated for 30 min at 4°C in the dark. These conditions caused oxidation of the vicinal diol groups that are present in the core saccharides, resulting in the generation of aldehyde groups (39,40). The oxidation was stopped by addition of glycerol (final concentration 15 mM). After 30 min, the oxidized LPS sample was dialyzed (dialysis membrane Spectra/Por cutoff: 3500 Da, Repligen (Waltham, Massachusetts, USA)) overnight at 4°C against 10 mM NaPO$_4$, 150 mM NaCl (pH 7.4). The fluorophore (Alexa647 hydrazide, NBD hydrazine, or TexasRed hydrazide) was dissolved in DMSO and added to the oxidized LPS to a final concentration of 2.5 mM. During an

overnight incubation the fluorophores covalently linked to the aldehydes at the core saccharides via hydrazone bonds. To remove unbound fluorophore, the sample was purified using a PD-10 Desalting Column (GE Healthcare, Chicago, Illinois, USA). Fractions containing the labeled LPS were centrifuged (280,000 × *g*, 3 h) and resuspended in 30 mL water. This step was repeated three times. After the last centrifugation, the LPS was resuspended in 1 mL water and stored at −20°C until usage.

In *S.* Typhimurium LPS, reactive vicinal diols are found in sugars of the core region, i.e., in heptose and 3-deoxy-D-manno-octulosonic acid residues. Enzymatic truncation of labeled LPS molecules with the specific bacteriophage depolymerase tailspike enzyme P22TSP specifically removes the O-antigen polysaccharide but leaves the core intact (41). P22TSP was purified after the protocol described by Miller et al. (42). When we treated GUVs containing labeled LPS with P22TSP to cleave off the O-antigen after the approach in (41), the membrane fluorescence signal showed no detectable changes compared with non-truncated samples. We thus conclude that the periodate oxidation step directed the fluorescence label to the core saccharide.

Depending on the application, LPS samples were labeled with different fluorophores chosen for most optimal performance considering the respective approach. TexasRed-labeled LPS was applied to determine LPS content in the membrane by comparing the membrane intensities with that of vesicles containing defined concentrations of TexasRed-labeled lipid. Via FCS and sFCS analysis, a labeling with maximum one fluorophore per LPS molecule was confirmed (for details on quantification of membrane intensities and labeling efficiency see Results and Discussion section on Assessing the LPS concentration in the membrane). LPS-Alexa647 molecules were employed in fluorescence recovery after photobleaching (FRAP) measurements together with NBD-PE lipids. FCS analysis showed that LPS molecules were labeled with one Alexa647 fluorophore (Fig. S3 *C*). The Alexa647 dye provides a larger spectral difference compared with the fluorescence spectra of NBD, avoiding unwanted fluorescence cross talk. To assess the membrane asymmetry via the quenching assay, LPS was labeled with NBD. The labeling ratio of LPS with NBD was not assessed. Considering the small contribution of the label to the LPS molecular weight, changes in LPS solubility and diffusion were not expected.

Preparation of symmetric and asymmetric GUVs

Lipid oil preparation

A thin lipid film was formed by drying solutions of lipids solubilized in chloroform (40 mM POPC or 1.15 mM NBD-PE) in a glass vial via evaporation under argon flow. The used volumes were adjusted depending on desired final lipid concentration (400 or 800 μM) and lipid oil volume. To remove all traces of chloroform the sample was dried for 1 h in a vacuum chamber. The dried lipids were dissolved in mineral oil. For better solvation, the sample was sonicated for 30 to 60 min in discontinuous mode. The mineral oil was added at low humidity (<10%) in a custom-built glovebox filled with nitrogen and monitored with a humidity gauge (Klimalogg Pro, TFA Dostmann, Wertheim-Reicholzheim, Germany). After overnight incubation in the dark at room temperature, the lipids were completely dissolved. When stored at 4°C, the lipid oil was used within 1 week.

Preparation of inner and outer aqueous solutions

Milli-Q Millipore water was used for the preparation of all aqueous solution. For the preparation of POPC-GUVs, an inner solution of 650 mM sucrose and an outer solution of 650 mM glucose were used. The preparation of GUVs with LPS in the outer leaflet (LPS-GUVs) required solutions containing glucose (650 mM), salt (10 mM NaCl, 10 mM MgSO$_4$, or 1–10 mM MgCl$_2$), 10 mM Tris-HCL (pH 7.6), LPS (10, 100, 200, or 500 μg mL^{-1}) and Alexa647-, TexasRed- (1.2 mol % of total LPS), or NBD-labeled LPS (6 mol % of total LPS). The concentration of the inner sucrose solution was adjusted to be isotonic to the outer aqueous solution (~700 mOsmol). Osmolarities were measured and adjusted with an osmometer (Osmomat

3000, Gonotec, Berlin, Germany). For the preparation of GUVs with LPS in the inner leaflet, an inner solution of 650 mM sucrose solution containing 10 mM $MgCl_2$, 10 mM Tris-HCl (pH 7.6), 100 μg/mL LPS, and 1.2 mol % TexasRed-labeled LPS was employed. The outer glucose solution was adjusted to be isotonic to the inner aqueous solution ($\sim$700 mOsmol). The high concentrations of the sugar solutions were chosen to ensure high yield as reported by Moga et al. (36).

GUV preparation via the inverted emulsion method

Symmetric POPC and asymmetric GUVs containing LPS in the inner leaflet. Outer solution (250 μL) was placed in a 1.5 mL Protein LoBind tube (Eppendorf, Hamburg, Germany), followed by 250 μL 800 μM POPC lipid oil (intermediate oil layer), which was layered on top. To form an interfacial monolayer, the sample was incubated for 3 h at room temperature. In the next step, 150 μL of a sucrose-in-oil emulsion was added on top and the sample was centrifuged for 10 min at 130 $\times$ g. The sucrose-in-oil emulsion was created by adding 5 μL inner solution (POPC: 650 mM sucrose; GUVs with LPS in the inner leaflet: 650 mM sucrose solution containing 10 mM $MgCl_2$, 10 mM Tris-HCl (pH 7.6), 100 μg/mL LPS, and 1.2 mol % TexasRed-labeled LPS) and 250 μL 400 μM POPC lipid oil in an additional Eppendorf tube and emulsifying via mechanical agitation along a standard Eppendorf tube rack for three times.
Asymmetric GUVs with LPS in the outer leaflet. Outer solution (250 μL) was placed in a 1.5 mL Protein LoBind tube, followed by 200 μL lipid-free mineral oil (intermediate oil layer), which was layered on top. To increase the amount of LPS at the water-oil-interface, the sample tube was mechanically agitated along a standard Eppendorf tube rack to form an oil-in-water emulsion. After incubation at room temperature for 30 min, the sample was centrifuged for 10 min at 600 $\times$ g and incubated for a further 3 h or overnight. In the next step, the sample was centrifuged for 10 min at 4500 $\times$ g to establish bulk phase separation of the oil and aqueous phase. A 50 μL amount of 400 μM POPC lipid oil was added to fill the gaps between the assembled LPS molecules at the water-oil-interface. After 15 min incubation at room temperature, 150 μL of a sucrose-in-oil emulsion was added on top. The sample was centrifuged for 10 min at 130 $\times$ g. The sucrose-in-oil emulsion was created by mixing of 5 μL inner solution and 250 μL 400 μM POPC lipid oil in an additional Eppendorf tube via mechanical agitation along a standard Eppendorf tube rack for three times.

PVA-assisted swelling of GUVs

PVA was dissolved in water by shaking at 95°C. Glass slides 7 $\times$ 2 cm were coated with 40 μL 40 mg mL^{-1} PVA solution and dried for 1 h at 35°C. A lipid solution (10 μL) of 4 mM POPC and DHPE-TexasRed (0.25 $\times$ 10^{-3}, 0.5 $\times$ 10^{-3}, 1 $\times$ 10^{-3}, or 2.5 $\times$ 10^{-3} mol %) were spread on the slides and dried under a stream of nitrogen followed by 1 h incubation in a vacuum chamber. The lipid-coated glass slides were assembled together with a Teflon spacer to form a swelling chamber (chamber volume was 2 mL) and filled with 650 mM sucrose solution. The GUVs were harvested after 10–20 min swelling duration. For imaging, 20 μL GUVs was added to 180 μL 650 mM glucose, 10 mM $MgCl_2$, 10 mM Tris-HCL (pH 7.6), and transferred to the observation chamber.

Confocal microscopy

Glass slides were incubated with 2 mg mL^{-1} β-casein for 15 min to coat their surface and avoid adhesion and bursting of the vesicles. Then they were rinsed with water and an observation chamber was assembled using a silicon spacer. Images of the GUVs were acquired using a confocal microscope (Leica microsystems TCS SP8, Wetzlar, DE) and a 40$\times$ oil immersion objective. Depending on the used fluorophores, different laser lines were employed: NBD was excited with an argon laser line at 488 nm and the emission signal was collected in the range 500–600 nm, TexasRed was excited using a diode-pumped solid-state (DPSS) laser at 561 nm, and emission collected in the range 600–700 nm and, Alexas647 was

excited with a HeNe laser at 633 nm and emission collected in the range 650–750 nm. For the z-stacks of the water oil interface, images in 0.5 μm steps were taken using a 25$\times$, 0.95 NA water objective.

Carboxyfluorescein permeability test

To check for the membrane permeability, carboxyfluorescein was dissolved (5 μM) in the sucrose (inner) solution for the formation of LPS-GUVs. The fluorescence in the vesicle lumen was recorded 2, 24, and 48 h after vesicle preparation. The carboxyfluorescein fluorescence was recorded by excitation using the 488 nm line of an argon laser and emission detected in the range 500–600 nm. To compare the fluorescence signals of the different days, the background fluorescence was subtracted from the lumen signal. For signal detection, circular regions of interest (ROIs) with diameters of 5 μm were created at the equatorial plane and placed in the vesicle lumen center and background (at the same height of imaging), respectively.

Quenching assay for membrane asymmetry estimation

The dithionite quenching assay (43) was used to determine symmetric or asymmetric distribution of NBD-PE- and NBD-labeled LPS. The assay was optimized to a robust and stable protocol by Leomil et al. (in preparation). In brief, unquenched GUVs were imaged at the equatorial plane and the membrane intensity was calculated using a custom-written MATLAB code (The MathWorks, Natick, MA). For symmetric lipid GUVs, a membrane composition of POPC and 0.5 mol % NBD-PE was employed. LPS-GUVs were doped with NBD-LPS. To quench the NBD fluorescence, 2.5 μL sodium dithionite stock solution of 0.1 M in 1 M Tris-HCl (pH 10) was added to a 97.5 μL GUV sample to a final concentration of 2.5 mM sodium dithionite. After 5 min the sample was diluted to a final dithionite concentration of 0.5 mM using equimolar glucose solution. The membrane intensity of the quenched GUVs was determined and compared with the unquenched membrane intensity. At least 12 GUVs were measured for each population. In the case of LPS-GUVs, a quencher concentration of 100 mM was employed to compensate for free NBD aggregates (left over from the labeling and due to inefficient washing). Higher dithionite concentrations were avoided to prevent membrane permeation. To verify that the membrane of the investigated vesicles is not leaky and that no quencher permeates it and quenches the inner leaflet, free Alexa647 was added to the outer solution to a final concentration of 200 nM and the dye fluorescence distribution across the membrane was monitored.

Membrane tubulation test upon vesicle deflation

To probe for the preferred membrane curvature, we examined the direction of tube formation in deflated vesicles. LPS-GUVs were loaded in a microfluidic chip (44) and flushed with a hyperosmolar solution. The lumen of the vesicles was 600 mM sucrose, while washing solution contained 650 mM glucose.

FRAP

FRAP was conducted to determine the diffusion coefficients of fluorescently labeled lipids (NBD-PE and DHPE-TexasRed) and LPS (TexasRed-LPS and Alexa647-LPS) in POPC- and LPS-GUVs. To avoid any movement, the GUVs were left to sediment to the bottom of microtiter plate wells (Corning, Corning, New York, USA) for $\sim$1 h. Two approaches in bleaching were employed as summarized next.

Spot FRAP measurements at the top of the GUVs

Spot FRAP was conducted to determine the diffusion coefficients of NBD-PE lipids and fluorescent LPS molecules. The confocal volume was

focused at the top of the GUV. Images (296 × 296 pixels) were recorded at bidirectional scan mode (1000 Hz) and with a pinhole at 1 Airy unit. Ten images at attenuated laser intensity (below 5%) were recorded followed by the photobleaching step. Photobleaching was performed using the maximum laser intensity for 526 ms (3 frames) through a circular ROI with a nominal radius of $r_n = 2.5$ μm. Afterward, the laser intensity was attenuated and the recovery was recorded for 18.35 s (70 frames). For LPS-GUVs that were labeled with NBD-PE and contained LPS-Alexa647, sequential scanning with the two laser lines at 561 and 638 nm was performed. The diffusion coefficient via FRAP measurements was calculated as described previously (45) (see also Lira et al. (46)):

$$D = \frac{r_e^2 + r_n^2}{8t_{1/2}}, \tag{1}$$

where r_e and r_n are the effective and nominal radius and $t_{1/2}$ is the halftime of fluorescence recovery. The nominal radius is the user-defined radius of the bleached area, while the effective radius describes its actual bleaching radius, which differs from r_n because of diffusion occurring already during photobleaching. The efficient radius r_e is derived from the line profile through the bleached area of the first post-bleached image and determined from fitting the line profile with

$$f(x) = 1 - K \exp\frac{-2x^2}{r_e^2}. \tag{2}$$

The halftime of fluorescence recovery $t_{1/2}$ is the time at which half of the recovered fluorescence is reached:

$$F_{1/2} = \frac{F_\infty + F_0}{2}. \tag{3}$$

The evaluation of the FRAP data was conducted with a custom-written MATLAB code (Fig. S1).

FRAP of one half of a GUV imaged at the equatorial plane

The second FRAP approach was conducted to investigate the diffusion behavior of NBD-PE lipids and fluorescent LPS molecules at the equatorial plane of LPS-GUVs and to compare them with each other. After bleaching one half of a GUV, the fluorescence in the bleached area recovered while the fluorescence intensity in the unbleached area decreased. The image recording was conducted until the fluorescence of both sides (bleached and unbleached) became equal due to diffusion. In the next step, the halftime of fluorescence recovery ($t_{1/2}$) is identified (see Eq. 3) from the recovery data. By recording the signal from the labeled lipid and LPS for one GUV at the same time, the ratio of the LPS and lipid recovery halftime $(t_{1/2})_{LPS}/(t_{1/2})_{NBD}$ can be directly assessed. This value describes the diffusion behavior of LPS molecules relative to that of lipid molecules in one GUV. Since these two parameters are recorded for the same GUV and converted to a relative ratio, the size of the GUV can be neglected.

The confocal microscope was focused at the equatorial plane of a selected GUV. Images (128 × 128 pixels) were recorded at bidirectional scan mode (1000 Hz) and with a pinhole at 1 Airy unit. Ten images at attenuated laser intensity (below 5%) were recorded followed by the photobleaching step. Photobleaching was performed using the maximum laser intensity for 1890 ms (15 frames) through a rectangular ROI, including one half of the GUV. Afterward, the laser was reduced to attenuated intensity and the recovery images were recorded until the signal equilibrated at both GUV halves. For LPS-GUVs that were labeled with NBD-PE and LPS-Alexa647, sequential scanning with the two laser lines 561 and 638 nm was performed.

Fluorescence correlation spectroscopy

To assess the molecular brightness and diffusion coefficient of free TexasRed dye and TexasRed-labeled LPS, fluorescence correlation spectroscopy (FCS) measurements were performed as described previously (47) on a confocal microscope (Leica Microsystems TCS SP8, Wetzlar, DE) using a 63×, 1.2 NA water immersion objective. Samples were excited with a 561 nm DPSS laser. Fluorescence was detected between 600 and 700 nm using a HyD SMD 2 detector in photon counting mode. The measurements were performed in spot acquisition mode for 3 × 12 times with 10 s intervals.

Leica files containing recorded photon arrival times were converted to intensity time series with time binning of 0.5 μs and subsequently analyzed using a custom-written MATLAB code. First, the autocorrelation function (ACF) of the fluorescence signal $F(t)$ was calculated as follows, using a multiple tau algorithm:

$$G(\tau) = \frac{\langle \delta F(t) \delta F(t + \tau) \rangle_t}{\langle F(t) \rangle_t^2}, \tag{4}$$

where $\delta F(t) = F(t) - \langle F(t) \rangle_t$. To avoid artifacts caused by rarely occurring LPS aggregates inducing single bright events, ACFs were calculated segment-wise (10 segments) and then averaged. Segments showing clear distortions were manually removed from the analysis. Next, a model for three-dimensional diffusion and Gaussian focal volume geometry (48),

$$G(\tau) = \frac{1}{N} \left(1 + \frac{T}{1 - T} e^{-\frac{\tau}{\tau_b}}\right) \left(1 + \frac{\tau}{\tau_d}\right)^{-1} \left(1 + \frac{\tau}{S^2 \tau_d}\right)^{-1/2}, \tag{5}$$

was fitted to the ACFs, resulting in parameter estimates of the diffusion time τ_d and particle number N. The exponential term accounts for photophysical transitions, e.g., to a triplet state, of an average fraction T ($0 \leq T \leq 1$) of fluorophores. The parameter τ_b was obtained from FCS measurements in TexasRed dye solutions and then fixed to the average value (around 8 μs) for the analysis of LPS-TexasRed samples. The structure parameter S was fixed to the value (typically around 5) obtained from daily calibration measurements of rhodamine B in water. From the diffusion time τ_d, the diffusion coefficient D was determined by $D = \frac{\omega_0^2}{4\tau_d}$. The beam waist ω_0 was determined from calibration measurements of rhodamine B in water, using the previously determined diffusion coefficient of $D_{RhoB} = 430$ $\mu m^2/s$ (49). Molecular concentrations c were calculated from the particle number N and the effective focal volume V_{eff} using $c = \frac{N}{V_{eff}N_A} = \frac{N}{\pi^{3/2}S\omega_0^3N_A}$, where N_A denotes the Avogadro number.

To determine the average labeling ratio, the molecular brightness $\frac{\langle F(t) \rangle_t}{N}$ (i.e., the average photon count rate emitted by each diffusing entity) was calculated and normalized to the average value determined for free TexasRed dye. For a labeling ratio of one, the brightness of the free dye and the labeled LPS molecule should be the same. All measurements were performed at room temperature.

Scanning FCS

To determine the molecular brightness and diffusion time of TexasRed-labeled LPS in LPS-GUVs and of TexasRed-DHPE in POPC GUVs prepared via PVA-assisted swelling, scanning FCS (sFCS) measurements were performed on a Zeiss LSM880 system using a 40×, 1.2 NA water-immersion objective. The molecular brightness was measured to compare the quantum yield of the TexasRed fluorophore when linked to LPS and a lipid (as in TexasRed-DHPE). The probes were excited with a 561-nm diode laser. Fluorescence was detected after passing through a long-pass 571 nm bandpass filter. Data acquisition and analysis were performed as described previously (48,50). In brief, line scans of 128 × 1 pixels (pixel size 41.5 nm) were performed perpendicular to the GUV membrane with a 291 μs scan time. A total of 500,000 lines were acquired (total scan

time ∼3 min) in photon-counting mode. Low laser power was used (∼24 μW) to minimize photobleaching and fluorescence saturation effect. Data were exported as TIF files, and then imported and analyzed in MATLAB using custom-written code (48,50). The analysis of the thus-obtained auto-correlation curves with a two-dimensional diffusion model resulted in the determination of the number of fluorophores in the confocal volume (N) and their apparent diffusion times. Furthermore, total fluorescence intensity at the GUV membrane and TexasRed-DHPE and LPS-TexasRed brightness were determined after background subtraction.

To confirm the labeling ratio, sFCS measurements were performed on the membrane of LPS-GUVs to assess the molecular brightness of LPS-TexasRed. By applying multiple bleaching cycles, the membrane intensity was reduced down to 10% of the initial value. If an LPS molecule were labeled with only one fluorophore, we would expect the molecular brightness to stay constant despite the total intensity becoming reduced. Whereas, if multiple fluorophores were linked to an LPS molecule, we would expect a decrease of the molecular brightness due to the bleaching of individual fluorophores in the same LPS molecule. To illustrate this, the bleached intensities of the different LPS membranes were normalized to the unbleached membrane intensity of the respective vesicle and plotted against the molecular brightness (Fig. S2 B). For better display, the molecular brightness of each bleaching cycle of one vesicle was normalized to the molecular brightness measured for the unbleached vesicle membrane.

Quantifying membrane fluorescence signal

Confocal cross-section images of spherical GUVs were recorded using constant settings (size, 1024 × 1024 px^2; scan speed, 400 Hz; bidirectional scanning mode; line average 3; pinhole, 1 Airy unit). The raw TIF images were loaded and analyzed using a custom-written MATLAB code (see Fig. S3). In brief, a Gaussian filter (kernel size, 2 pixels) was applied and areas of the image that should not be considered for the further analysis (e.g., lipid aggregates, neighboring GUVs, etc.) were excluded. After selection of the vesicle center, a radial line profile was calculated. By cubic curve fitting, the baseline of the line profile was identified. After subtraction of the baseline, the area of the line profile's peak was computed. The peak area was used to estimate to the average concentration of fluorophore in the vesicle membrane (Fig. S3).

RESULTS AND DISCUSSION

Due to the unique characteristics of LPS, and especially smooth LPS, their incorporation into an asymmetric membrane is non-trivial and required extensive modification of the inverted emulsion technique (35,36). This protocol is based on the stepwise formation of two separate leaflets to build the final GUVs. The leaflets derive from monolayers of amphiphilic molecules assembled at the surface of aqueous droplets in oil (inner leaflet) and at a planar water-oil interface (outer leaflet). By application of centrifugal force, the droplets cross the interface combining the two monolayers to leaflets of a complete vesicle bilayer. The self-assembly of amphiphiles, such as lipids at water-oil interfaces, is a spontaneous process that is governed by shape anisotropy and enthalpic forces (hydrogen-bonds and π-stacking) and is characterized by high affinity of the lipids for the interface (51). However, the interaction of LPS molecules with water-oil interfaces is less favorable due to the micellar structures that LPS form in aqueous solutions (7). The monolayer self-assembly of charged polymeric amphi-

philes is characterized by slow kinetics, limited by conformational and packing constraints (52). Due to these reasons, the original method of the inverted emulsion technique (35,36) yielded vesicles with very low levels of LPS incorporation (as discussed later and shown in Fig. 3 A). Longer incubation times of LPS with the water-oil-interface did not produce substantial improvement. The same held true for a large variety of modifications we explored in terms of different centrifugation speeds, used oils, volume ratios, and LPS and sugar concentrations. Thus, we attempted to optimize the protocol by introducing a new step. In our study we used smooth LPS isolated from *S.* Typhimurium (thereafter referred to as LPS) to prepare the outer GUV leaflet and the lipid POPC for the inner one. Fluorescently labeled LPS was used to monitor LPS incorporation into the GUV membranes or the water-oil interface, and fluorescent lipids were used to monitor lipid distribution and mobility.

New emulsification/incubation step leads to successful LPS-GUV preparation

We speculated that the crucial deficiency of the inverted emulsion protocol is the poor adsorption of LPS from the aqueous phase to the water-oil interface. Therefore, we aimed at increasing the surface area of the water-oil interface and reducing the diffusion distance of LPS to this interface, which we expected to help better assemble the outer, LPS-rich vesicle leaflet. To achieve both of these aims, we introduced the new step of emulsification of lipid-free mineral oil in LPS-containing aqueous solution and hence provided an increased interface area for more LPS molecules to adsorb (illustrated in the red box in Fig. 1). Furthermore, we assume that this additional step increases the probability of an encounter between the dispersed oil droplets and LPS micelles, causing "spreading" of LPS molecules and mixing of material, originating from the micellar structures, onto the emulsion droplets. Subsequent centrifugation leads to restoring the continuous water-oil interface with increased number of assembled LPS molecules. The processes during this additional emulsification/centrifugation step and the complete method are sketched in Fig. 1. To probe the validity of this speculated mechanism of enriching the water-oil interface by additional emulsification, we examined the equilibrated interface (Fig. 1 C) with z-stack confocal imaging (Fig. 2). Simple incubation of the LPS solution with mineral oil (Fig. 1 A) did not lead to a detectable monolayer formation at the water-oil interface; z-scans only showed homogenous distribution of labeled LPS in the bulk (Fig. 2 A). The emulsification of LPS solution and mineral oil and subsequent centrifugation led to accumulation of LPS molecules (Fig. 2 B) at the interface; see line profiles indicating the absence or presence of increased LPS content at the interface (Fig. 2). However, not all LPS molecules assembled at the interface, as some remained in the bulk. Note that, even after this step, the water-oil interface was
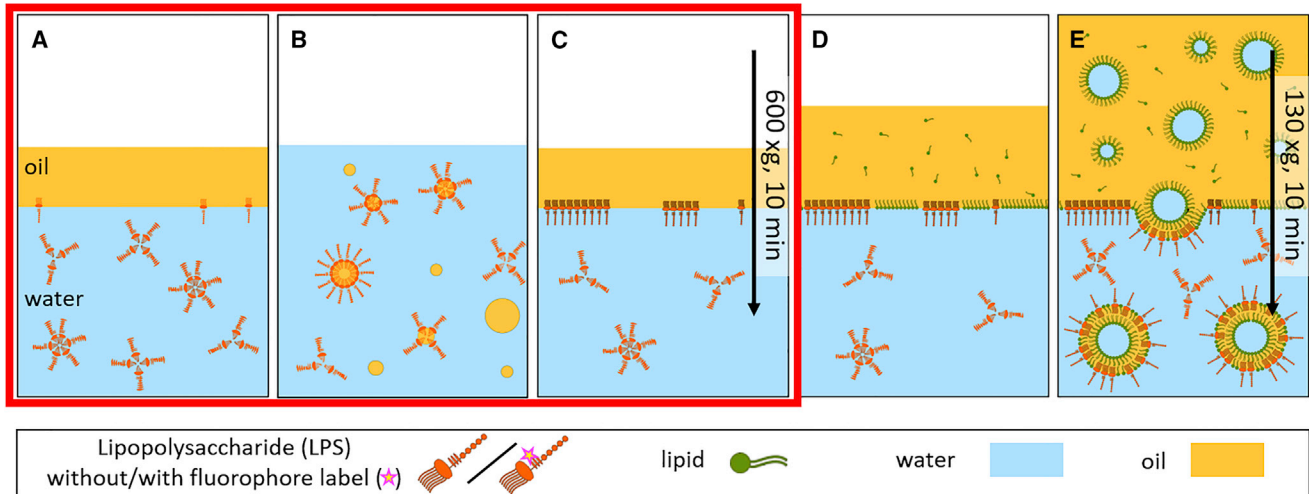
FIGURE 1 Schematic illustration of the preparation of bacterial membrane mimetic system, namely asymmetric LPS-containing GUVs, using a modified inverted emulsion protocol. (*A* and *B*) To create the outer leaflet of the GUV, an LPS monolayer has to be formed at a water-oil interface. In aqueous solutions, the LPS molecules form micellar structures, which hinder the assembly of LPS molecules at the water-oil interface. To assist the LPS monolayer formation, a glucose solution containing LPS is emulsified in lipid-free oil increasing the area of the water-oil interface and reducing the diffusion time of LPS to such interface. (*C*) A continuous water-oil interface is re-established by centrifugation at $600 \times g$ for 10 min. During an interfacial incubation time of 3–19 h allowing for conformational sampling and rearrangement, the LPS molecules form patches at the interface. (*D*) To fill the gaps between the LPS molecules, a lipid oil is layered on top of the sample. During an incubation time of 15–30 min, lipid molecules assemble at the free spaces at the water-oil interface. (*E*) In parallel, a sucrose solution is emulsified in lipid oil and applied on top of the sample. The formed sucrose droplets in oil provide the lumen and the inner leaflet of the GUVs and the lipids assembled at the droplet-oil interface form the inner GUV leaflets. During centrifugation ($130 \times g$, 10 min), the denser sucrose droplets cross the LPS monolayer and lead to the formation of a complete bilayer and thus to the formation of LPS-doped asymmetric GUVs. LPS incorporation was monitored using a fraction of fluorescently labeled LPS, in which the fluorophore is located at the core saccharides, as illustrated in the legend. To see this figure in color, go online.

not homogenously covered but exhibited patches of enhanced LPS fluorescence signal (Fig. S4 as sketched in Fig. 1 C). To ensure a sufficient vesicle yield, the gaps between the LPS-rich patches at the interface were filled up by POPC molecules by layering lipid oil on top of the sample (Fig. 1 D). Then, following the conventional steps in the protocol, a sucrose-in-oil emulsion stabilized by lipids is added on the sample, followed by centrifugation (Fig. 1, E).

The LPS GUVs produced with this modified protocol showed heterogeneous size distribution, with diameters ranging from 5 to 45 μm with a mean of 19 $\pm$ 8 μm (Fig. S5). This size distribution was similar for all tested preparation conditions. The vesicles appeared stable for at
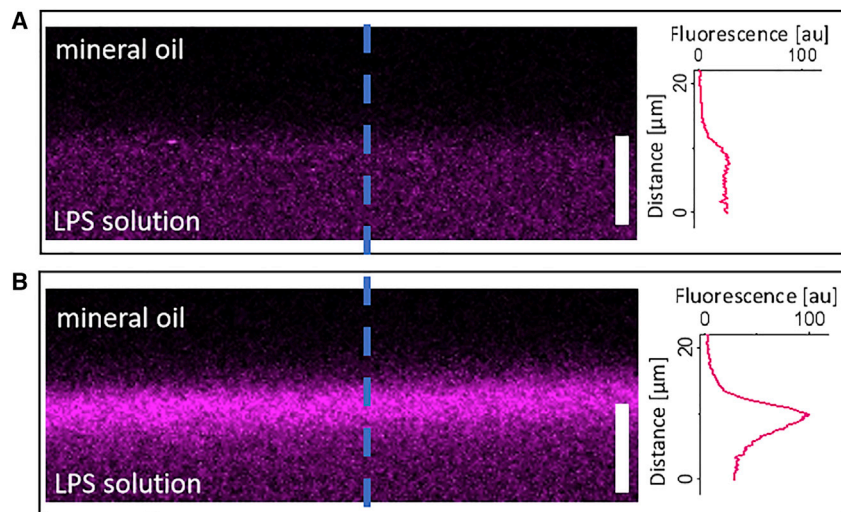
FIGURE 2 Imaging and analysis of the water-oil interface and formation of LPS monolayer. Side view rendering from a confocal microscope z-stacks (0.5 μm steps) show the accumulation of LPS molecules (labeled with Alexa647, *magenta*) at the water-oil interface. A line profile is measured along the dashed blue line and plotted in the right panels to show the distribution of LPS-Alexa647. The scale bars correspond to 10 μm. (*A*) Water-oil interface after 1 h incubation of 25 μL LPS-containing aqueous solution with 50 μL lipid-free mineral oil. The line profile on the right shows that no detectable LPS monolayer has formed. (*B*) After the new additional emulsification/centrifugation step (as sketched in Fig. 1, *A–C*) using LPS-containing aqueous solution and lipid-free mineral oil, a continuous water-oil interface and an LPS monolayer was formed. LPS-containing solution (25 μL) was mixed with 50 μL mineral oil via mechanical agitation once along an Eppendorf rack. The emulsion was transferred in a well plate and centrifuged at $90 \times g$ for 10 min. The z-stack was recorded directly after the centrifugation. The assembly of the LPS molecules at the interface is demonstrated by the peak in the line profile in the right panel. To see this figure in color, go online.

least 2 days showing no leakage of encapsulated carboxy-fluorescein dye (Fig. S6 A) nor loss of LPS signal (monitored with fluorescently labeled LPS-Alexa647) when washed in isotonic glucose (Fig. S6 B). Between 90 and 98% of all GUVs showed LPS incorporation. This is a very high yield compared with samples obtained without the emulsification step, which showed only very low levels of LPS incorporation ($\sim$2.5% of all GUVs; compare panels in Fig. 3, A, B, and F). GUVs containing LPS displayed an increased fluorescence signal at the membrane that was absent in GUVs without LPS (see Fig. 3, C–E). The background fluorescence around the vesicles was caused by free unincorporated LPS-Alexa647 and/or free Alexa647 dye molecules that were not completely removed during the LPS labeling process. The LPS surface coverage of the GUVs obtained with the new protocol also showed variations from vesicle to vesicle.

To probe whether the new emulsification step alters lipid packing and/or introduces differential stress in the membrane (53), we examined the vesicle morphology upon deflation and measured lipid diffusion in POPC lipid GUVs prepared with electroformation, the standard inverted emulsion approach, and the modified protocol introduced here. Vesicle deflation in all different samples yielded prolate or multisphere GUVs as expected for vesicles, with sucrose/glucose asymmetry across the membrane (54), and the FRAP experiments showed similar diffusivity regardless of the protocol used for preparation (Fig. S7).

To achieve a higher LPS fraction in the outer leaflets, the used LPS concentration had to be high enough to cover large areas of the water-oil interface. In the given experimental set-up, a concentration of 100 μg mL^{-1} proved to be optimal, as higher concentrations (200 μg mL^{-1}) did not lead to higher yield of LPS GUVs. Lower concentrations (10 μg mL^{-1}) still resulted in high fractions of LPS GUVs, but at the expense of the overall GUV yield (Fig. 3 F).

Divalent cations have been shown to be critical for LPS-doped membrane stability and maintenance of bilayer asymmetry in solid-supported bilayers (6). They bridge the negative charges of the phosphate groups at the LPS inner cores (55) and prevent mutual electrostatic repulsion. Divalent cations, such as calcium ions, affect also LPS-free membranes; exhibiting on the one hand tension increase and spontaneous-curvature effects upon adsorption to GUVs made of charged lipids (56–58), but, on the other hand, also stabilizing such membranes upon poration (59). Calcium ions have been also shown to induce substantial conformational changes in LPS monolayers (60). Thus, we assumed that divalent cations would facilitate the formation and stability of the LPS monolayer in the preparation step of our protocol. The optimal concentration of divalent cations should be higher than the minimum concentration required to bridge the negative charge, but still low enough to reduce vesicle-vesicle adhesion caused by divalent cations (8). For the chosen settings, a concentration of 10 mM was found optimal (Fig. 3 F). Monovalent cations, such as sodium ions, cannot bridge the negative
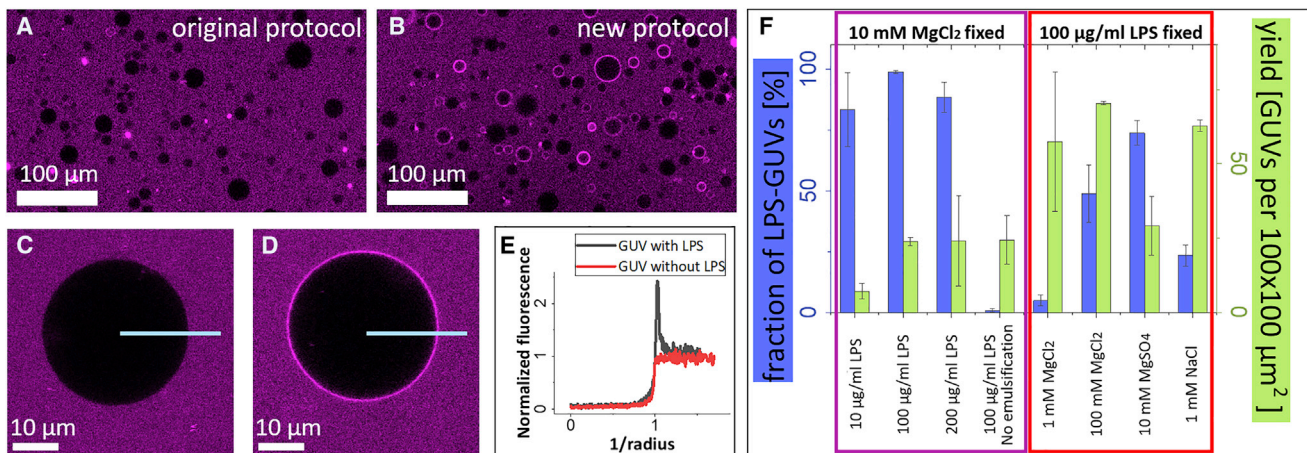

FIGURE 3 Incorporation of LPS in asymmetric GUVs and vesicle yield. LPS incorporation in the GUV membrane was quantified from the fluorescence signal of LPS labeled with Alexa647 dye (*magenta signal*). (A and B) LPS-GUV yield improves dramatically after implementation of the new emulsification/incubation step. Confocal images illustrating the GUV population in samples that were prepared without (A) and with (B) the emulsification step. The images illustrate the heterogeneity of the GUVs in size and LPS incorporation. With the emulsification step, the yield of LPS-GUVs showing enhanced signal at the membrane increased from 2.5 to 90–98%. (C) GUV without LPS-incorporation. (D) GUV with LPS incorporation. (E) Radial intensity profiles of the vesicles in (C and D). Successful LPS incorporation in the membrane is exhibited by a peak in the fluorescence. The fluorescence intensity data were normalized by the signal in the GUV surroundings and distance is plotted in units of the vesicle radius. (F) Fraction of LPS-GUVs (*blue bars*) and overall GUV yield (*green bars*) were tested for different preparation conditions: LPS concentration, MgCl$_2$ concentration, usage of NaCl or MgSO$_2$ instead of MgCl$_2$, absence of the new emulsification step. All samples had an interfacial incubation time of 1 h. Magenta rectangle: LPS concentrations were varied while 10 mM MgCl$_2$ was fixed. Red rectangle: salt conditions were varied while the LPS concentration was fixed to 100 μg/mL. Three replicates of each condition were prepared and 10 random images (100 $\times$ 100 μm^2) per replicate were recorded. The error bars show the standard deviation. The images were evaluated by manually counting the total number of GUVs present (only vesicles with diameter larger than 10 μm were considered) and which of them show any LPS incorporation. To see this figure in color, go online.

charge of neighboring LPS molecules, but they can screen it and thus avoid electrostatic repulsion. However, the use of NaCl resulted in a lower fraction of LPS GUVs compared with the conditions when $MgCl_2$ or $MgSO_4$ were used. Replacing $MgCl_2$ by $MgSO_4$ resulted in similar (albeit lower) fraction of LPS-GUVs. Chloride ions are less kosmotropically active compared with sulfate ions (61). Due to the stronger stabilization of hydrophobic interactions (61), sulfate ions might promote aggregation of LPS molecules and thereby adversely affect the monolayer assembly at the water-oil interface. Therefore, $MgCl_2$ was chosen as optimal salt type and used in further experiments.

LPS is asymmetrically distributed across the membrane

The preparation protocol as sketched in Fig. 1 suggests that LPS should be distributed exclusively at the outer GUV leaflet. However, we cannot monitor the production process directly to see whether LPS has flipped/migrated to the inner leaflet either because of improper resealing, or leakage, or

stress in the membrane. To probe the actual distribution of LPS in the membrane, a quenching assay was performed based on the use of NBD-labeled LPS or PE lipids. The membrane-impermeable quencher sodium dithionite, added externally, irreversibly quenches the NBD fluorophores in the outer leaflet of the vesicle membrane. The fluorophores in the inner leaflet are not affected (Fig. 4). In vesicles with symmetrically distributed NBD, a fluorescence loss of 50% occurs which we confirmed on symmetric GUVs prepared with POPC and NBD-PE lipids, see data in green in Fig. 4 B. Vesicles with an asymmetric NBD distribution, either on the inside or outside, should show no loss or a complete loss of the fluorescence signal, respectively. LPS GUVs with NBD-labeled LPS in the outer leaflet lost $79 \pm 10\%$ of the original fluorescence (Fig. 4, data in *magenta*), indicating an asymmetric LPS distribution. This decrease in fluorescence indicates that not all fluorophores could be quenched. In addition to the above-listed reasons, this result could be caused by protected fluorophores at the inner leaflet or not fully efficient quenching. More importantly, in the case of LPS GUVs, free LPS-NBD might
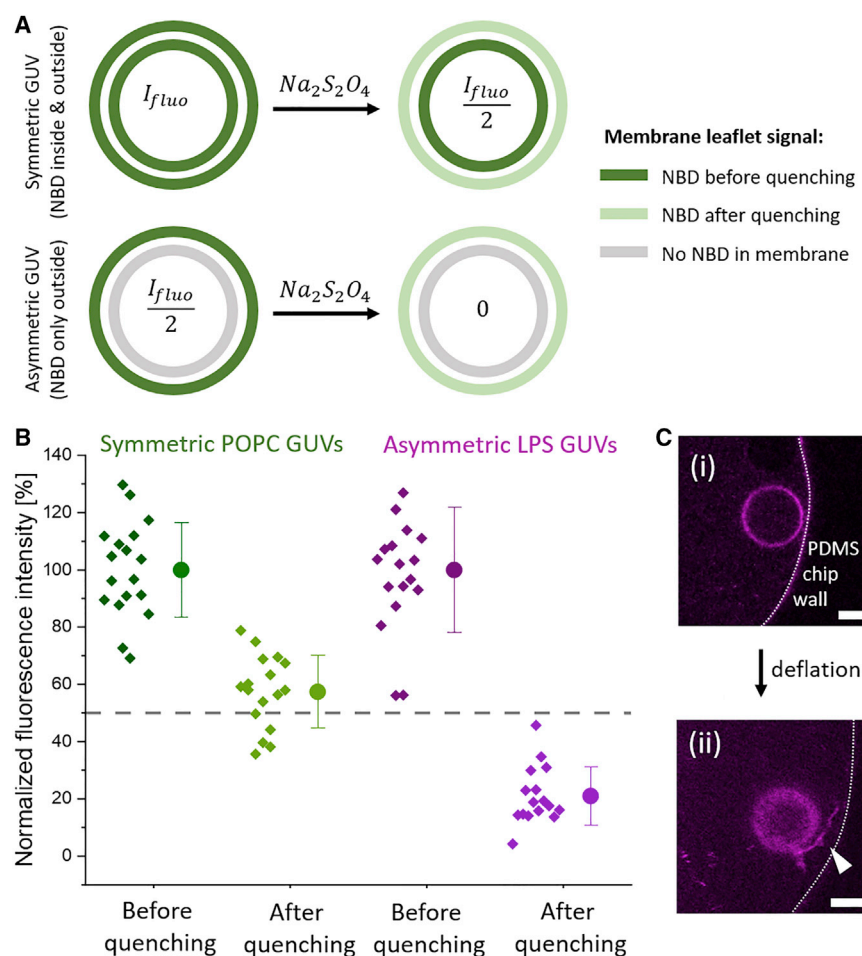

FIGURE 4 LPS is preferentially distributed at the outer GUV leaflet as shown by quenching assay and vesicle tubulation. (*A*) Schematic illustration of the mechanism of the NBD-quenching assay. The NBD signal from the labeled molecule is quenched by sodium dithionite ($Na_2S_2O_4$). Because sodium dithionate does not permeate the membrane, only fluorophores at the outer leaflet are quenched. For symmetric dye distribution the initial fluorescence signal (I_{fluo}) decreases by 50%. Asymmetric GUVs that incorporate the NBD label only in the outer leaflet show a complete loss of fluorescence, while GUVs with the NBD label in the inner leaflet only retain their fluorescence. (*B*) The initial (not quenched) NBD fluorescence intensities for NBD-PE in POPC GUVs (*green*) and LPS-NBD in LPS-GUVs (*magenta*) were recorded and normalized to 100% after subtracting background signal. After incubation of the POPC and LPS-GUVs with the quencher, the fluorescence dropped by $43 \pm 12\%$ and $79 \pm 10\%$, respectively. This indicates symmetric fluorophore distribution for POPC GUVs and an asymmetric fluorophore distribution for LPS GUVs. Each point represents one measurement on a different GUV. The dashed reference line refers to 50% of initial fluorescence intensity; the mean and standard deviations are displayed to the right of the data. (*C*) Single-vesicle deflation in a microfluidic chip leads to outward tube formation. An LPS GUV was washed with hyperosmolar glucose solution in a microfluidic chip; the channel boundary (*dashed white line*) in which the vesicle was trapped is well visible in fluorescence (i) due to adsorbed free LPS, which is washed away with the deflation step in (ii). Before the deflation the vesicle is spherical and free of defects and

protrusions. After deflation (ii), the GUV formed an outward tube (see *arrowhead*), indicating asymmetric distribution of the LPS molecules. The focal plane was changed to visualize the tube better. The scale bars correspond to 5 μm. To see this figure in color, go online.

be still present in the vesicle exterior, which could exhaust a fraction of the quencher reducing the quenching efficiency.

In addition to fluorophore quenching, membrane asymmetry can be verified via membrane deformations. Asymmetric transmembrane distribution of molecules with large headgroups has been shown to lead to tubulation in giant vesicles upon deflation (62,63). These tubes are stabilized by non-zero membrane spontaneous curvature (64), which can be generated by various types of asymmetry (63,65–71). Even if the two leaflets of the membrane are tensionless, small asymmetry in the molecule distribution can lead to significant spontaneous curvature (72). In the case of GUVs prepared with a method based on the sequential assembly of monolayers at the water-oil interface, one could expect that the residual oil molecules retained in the hydrophobic core of the bilayer can act as an agent reducing the leaflet tension, as cholesterol does with its frequent flip-flop (72). However, the asymmetric LPS distribution in our systems can be expected to result in large spontaneous curvature of the GUVs. Because LPS is in the outer leaflet, the spontaneous curvature should be high and positive. The sugar asymmetry characteristic for our system should also generate positive but small spontaneous curvature with a magnitude of about 1 μm^{-1} (54). Thus, depending on the LPS coverage, we expected the formation of outward tubes that are thin (with diameters below optical resolution) for vesicles with higher LPS coverage or 1–2 μm thick for vesicles at lower LPS coverage. The necessary condition for these morphologies to occur is that the vesicles have excess area available for shape changes. To allow this, we deflated the vesicles with hyperosmolar solutions (see Materials and methods section on Membrane tubulation test upon vesicle deflation). When this is done in the bulk, many vesicles could exhibit tubulation; however, the initial morphology of the vesicle is unknown. To be able to follow a single vesicle with a known shape (sphere), we deflated individual vesicles while monitoring their shape change in a microfluidic device described earlier (44). One example of such a

vesicle is provided in Fig. 4 C. After deflation, the initially spherical and tube-free vesicle develops a long thin outward tube. Vesicles with lower LPS coverage were observed to develop thicker tubes as expected (Fig. S8). These observations confirm the asymmetric distribution of LPS in the obtained GUVs and point to an approach for modulating the membrane morphology based on this asymmetry. In contrast, GUVs with LPS localized at the inner leaflet developed inward pointing tubes after deflation (Fig. S9), further corroborating this concept.

Assessing the LPS concentration in the membrane

As indicated above, the vesicles showed heterogeneous LPS coverage demonstrated by the variations in the signal from fluorescently labeled LPS in the membrane (Fig. 3). To determine the LPS coverage on individual GUVs, we used a calibration fluorophore standard. The membrane intensity of LPS-GUVs containing TexasRed-labeled LPS was compared with the membrane intensity of POPC-GUVs prepared with distinct concentrations of TexasRed-labeled DHPE lipids (note that the POPC vesicles used for the calibration were prepared using the method of PVA-assisted swelling (22) to avoid uncertainties regarding the fluorophore fraction incorporation that could be expected of preferential partitioning to the oil-water interface). In brief, the total membrane intensity of different GUVs in the reference samples were measured (as described in Materials and methods section on Quantifying membrane fluorescence signal and Fig. S3) and converted into a single leaflet intensity by dividing by the factor 2. Plotting the membrane leaflet intensity as a function of the molar fraction of TexasRed-DHPE in the corresponding reference samples reveals a linear relation (Fig. 5 A) described as $n_{TR-DHPE} = (I - 0.06)/33.2$, where $n_{TR-DHPE}$ is the mole fraction of TexasRed-DHPE (in mol %) in one vesicle leaflet and I is the membrane intensity (in arbitrary units). This linear fit
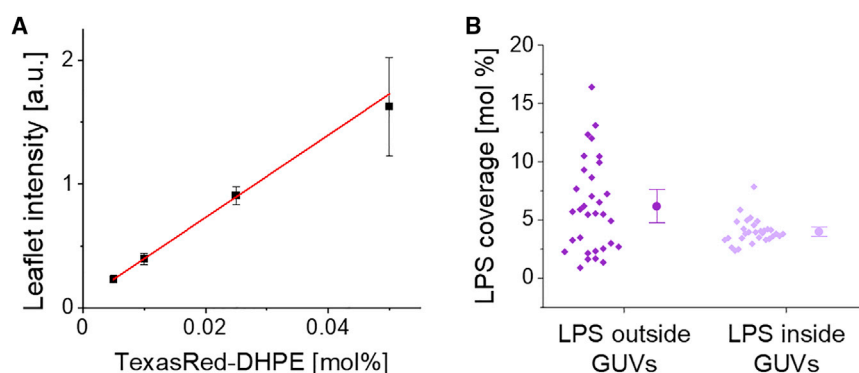
FIGURE 5 Membrane intensity calibration and calculation of LPS incorporation in asymmetric vesicles. Experiment and recording conditions are kept constant. (*A*) The membrane intensities of POPC-GUVs doped with varied TexasRed-DHPE concentrations and their respective membrane signals showed a linear relation, which was used as calibration of leaflet intensity and TexasRed membrane concentration. Fifteen vesicles for each TexasRed-DHPE concentration were imaged. (*B*) The concentration of TexasRed-labeled LPS in the inner or outer leaflet of the membrane of asymmetric GUVs, respectively, is calculated via the fit function of the calibration data and correction factors for LPS labeling efficiency and fluorophore quantum yield. The mean and the standard deviations are displayed on the right of the data. To see this figure in color, go online.

is used to determine the molar fraction of TexasRed fluorophore in the outer or inner leaflet of the LPS GUVs from the measured intensity. However, to perform this conversion, we needed to know how many TexasRed groups were bound to one labeled LPS molecule. We used two approaches to find out. First, FCS experiments measuring number and brightness of LPS-TexasRed and free TexasRed in bulk showed that the molecular brightness of LPS-TexasRed is slightly lower compared with that of the free dye. This indicated that LPS was labeled with a maximum of one fluorophore per molecule (compare Fig. S2 A). This measurement, however, does not address potential difference between the quantum yield of the TexasRed fluorophore when free or bound to LPS. Thus, we used a second approach, namely, by performing sFCS measurements on the membrane of LPS-GUVs (48,50). By applying multiple bleaching cycles, the membrane intensity was reduced down to 10% of the initial value (for more details see Materials and methods section on sFCS). Since the molecular brightness stayed constant during the bleaching cycles (Fig. S2 B), the labeling of approximately one fluorophore per LPS molecule was confirmed. Therefore, it can be assumed that the fluorophore concentration in the LPS-GUV membrane is equal to the concentration of LPS-TexasRed in the membrane. Finally, to correct for the difference in quantum yields of TexasRed when bound to LPS compared with when bound to DHPE, we performed molecular brightness analysis via sFCS experiments. The data revealed that LPS-TexasRed exhibits a 15% lower quantum yield than TexasRed-DHPE (data not shown). Therefore, the molar concentration of LPS-TexasRed, as deduced from the calibration curve (Fig. 5 A) was correspondingly corrected, i.e., $\frac{n_{TR-DHPE}}{1-0.15}$. Since only 1.2% of the total LPS for vesicle preparation was labeled with TexasRed, the total LPS concentration in the membrane was additionally corrected as $\frac{n_{TR-DHPE}}{1-0.15}\frac{1}{0.012}$.

With the approach described above, we assessed the LPS fraction in GUVs in the outer leaflet (LPS-outside GUVs) and in GUVs with LPS in the inner leaflet (LPS-inside GUVs). In the outer leaflet, 1–16 mol % (16–79 wt %) LPS were incorporated, while only 2–7 mol % (28–60 wt %) LPS could be incorporated in the inner leaflet (Fig. 5 B). These fractions describe the LPS fraction in the respective leaflet. Presumably, the lower LPS content in the LPS-inside GUVs is caused by the altered preparation protocol (Fig. S10). For this system, the LPS monolayer is formed by emulsification of the inner aqueous solution with lipid mineral oil. The general incubation time of this emulsification is much shorter and the presence of POPC lipids during interface incubation led to competition in terms of amphiphilic arrangement at the interface. In contrast, LPS-outside GUVs were incubated longer and without the presence of POPC molecules.

By measuring the LPS concentration, we further probed the effect of monolayer incubation times (Fig. 6 and step (C) in Fig. 1): 1 h, 3 h, and overnight (~19 h) were tested
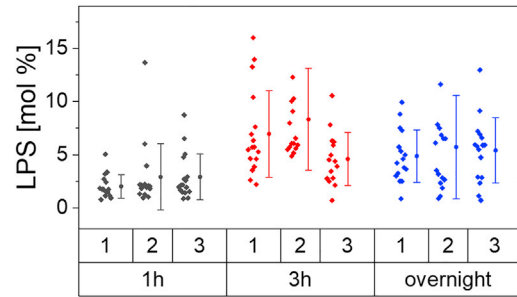

FIGURE 6 LPS incorporation after application of different incubation times for monolayer incubation (Fig. 1 C). Incubation times of 1 h, 3 h, and overnight (~19 h) were tested and the individual LPS concentrations in the vesicle membrane were calculated. Three replicates of each condition were prepared (numbers 1, 2, and 3) and 16 random vesicle images per replicate were recorded. The mean and the standard deviations are displayed to the right of the data. To see this figure in color, go online.

for the amount of LPS incorporation using fluorescence imaging. In all three cases, every GUV in the samples showed LPS incorporation in the membrane, but the membrane intensities and thus LPS coverage varied. An incubation time of 1 h resulted in only 1–4 mol % LPS in the membrane on average, while 3 h or more allowed LPS incorporation yields in the range of 1–16 mol % (Fig. 6).

Higher LPS coverage slows membrane diffusion

Compared with phospholipids, LPS molecules exhibit enhanced lateral interactions due to three structural properties of the molecule. (i) As mentioned above, the bridging of the negatively charged phosphate groups by divalent cations leads to strong electrostatic interaction between LPS molecules. In the presence of Mg^{2+} ions, Takeuchi and Nikaido observed the existence of pure LPS domains (stable for days) without mixing with phospholipid molecules (73). Several studies have shown that LPS molecules in membranes adopt a gel-like state in the presence of divalent cations, which reduces the mobility of the individual molecules and LPS domains (2,6,74–76). (ii) The presence of seven fatty acyl chains in the lipid A portion compared with only two in phospholipids provides a greater surface area, allowing for stronger hydrophobic interactions between the lipid A portions of the LPS molecules (2). (iii) Smooth LPS has been shown to have higher melting temperature than truncated LPS molecules (75,77,78), indicating an additional contribution to the lateral interactions between the elongated sugar chains. These interaction characteristics are missing in phospholipids.

Employing spot FRAP measurements (see Materials and methods section on Spot FRAP measurements at the top of the GUVs and Fig. S1 for details) we explored how these enhanced interactions affect diffusivity in the membrane of asymmetric LPS-GUVs. Both lipid and LPS diffusion were explored and compared with lipid mobility in LPS-free membranes. The diffusion coefficient of Alexa647-labeled LPS (4.3 ± 0.8 μm^2 s^{-1}, *magenta* data in

Fig. 7 A) was found to be 20% lower than the lipid diffusion coefficient ($5.3 \pm 1.3 \, \mu m^2 \, s^{-1}$, *light green* data in Fig. 7 A) in the membrane of LPS GUVs. Note that, because of the presence of lipids on both sides of the membrane, the diffusion coefficient that was measured for the lipid signal originated from both the inner and outer leaflet.

This decrease is understandable considering the large molecular size of LPS. We also compared the lipid diffusion in LPS-free with LPS-doped GUVs. A two-group *t*-test showed that the mean diffusion coefficient of NBD-PE lipids in POPC GUVs and LPS-GUVs are not significantly different (*light* and *dark green* data in Fig. 7 A). Presumably, the relatively low fraction of LPS in the membrane is not sufficient to slow down lipid diffusion significantly also considering that NBD-PE was present in both leaflets, in the outer LPS-doped one and in the inner LPS-free one where diffusion is unhindered. We cannot exclude that diffusion of labeled lipids can be different from that of the unlabeled lipid (POPC), but considering the large difference of the molecular weights of the labeled lipid and LPS we expect that the LPS versus lipid behavior should be qualitatively correctly reflected by our diffusion measurements.

In view of the large scatter in the data for the LPS membranes, we questioned whether the diffusion coefficients in individual vesicles correlate with their specific LPS surface coverage. The FRAP experiments revealed that increasing LPS concentration in the membrane lowers LPS diffusivity (Fig. 7 B). This finding corroborates previously reported data on LPS mobility in symmetric membranes: Kubiak et al. speculated that higher LPS coverage leads to the formation of gel-like LPS domains that are below the resolution of confocal microscopes and which caused the decrease in the measured diffusion coefficients (17).

Due to the slow diffusion and relatively low coverage, spot FRAP measurements were not possible on all LPS-GUVs. During the recording of the post-bleach images, back-diffusing LPS-Alexa647 molecules were photobleached, preventing the recording of a fluorescence recovery of the bleached area and hindering data acquisition (see Fig. S1 D). Therefore, we developed a single-vesicle essay in which

we assess the different diffusion behaviors of POPC lipids and LPS by bleaching half of a GUV at the equatorial plane (for details see see Materials and methods section on FRAP of one half of a GUV imaged at the equatorial plane). This adapted protocol allows following the fluorescence recovery without photobleaching the back-diffusing molecules by reducing the laser power. In brief, one half of the LPS GUV was bleached at the equatorial plane and the recovery curves for NBD-PE and LPS-Alexa647 were recorded simultaneously. The ratio of the LPS and lipid recovery halftimes $(t_{1/2})_{LPS}/(t_{1/2})_{NBD-PE}$ was determined and used to describe the diffusion behavior of LPS molecules relative to that of lipid molecules in one GUV (Fig. 8). Since these two parameters were recorded for the same GUV and converted to a relative ratio, the size of the GUV does not play a role. We find that the diffusion of LPS is by a factor of 2.33 ± 0.50 slower than that of lipids in the same GUVs. This result is in excellent agreement with sFCS measurements, which showed that the diffusion time of LPS-TexasRed in LPS membranes is 2.23 times higher than the diffusion time of TexasRed-DHPE in POPC GUVs prepared via PVA-assisted swelling (Fig. S11 B). This agreement emphasized the validity of our approach based on half-GUV FRAP.

Summary and conclusions

In this work we report the production of a vesicle-based model of the OM of *S.* Typhimurium using a novel inverted emulsion method. In contrast to the complex microfluidic method that achieves asymmetry leaflets, this technique is applicable in many laboratory settings, as only a benchtop centrifuge and sonication bath are required.

The presented protocol allowed the production of asymmetric GUVs containing LPS either in the outer (1–16 mol %, corresponding to 16–79 wt %) or inner membrane leaflets (2–7 mol %, corresponding to 28–60 wt %), respectively. The asymmetric distribution of LPS was confirmed with a quenching assay. Furthermore, we demonstrated that, upon deflation, the vesicles exhibit membrane tube formation, whereby the tubular structures are stabilized
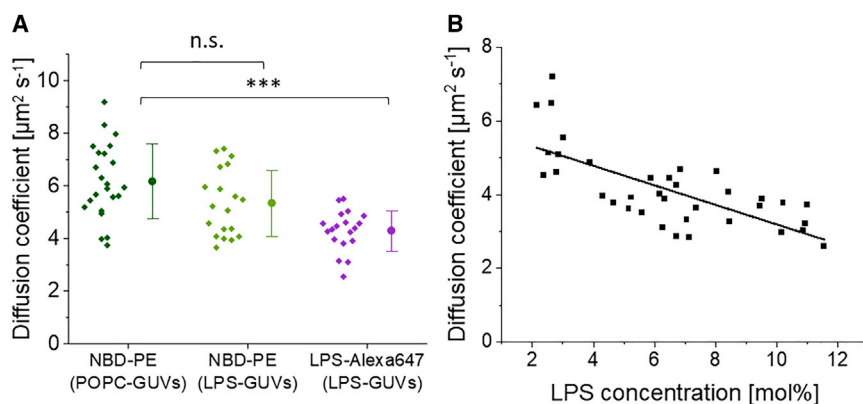

FIGURE 7 Diffusion of labeled lipids and LPS in POPC- and LPS-GUVs measured via spot-FRAP. In both panels, each point represents one measurement on a different GUV. (*A*) Diffusion coefficients measured for NBD-PE in POPC GUVs (*dark green*) and in LPS-GUVs (NBD-PE present in both leaflets, *light green*), and LPS-Alexa647 (*dark magenta*) in LPS-GUVs. The diffusion coefficients of NBD-PE and LPS-Alexa647 are significantly different (two-sample *t*-test, p ≤ 0.001). The mean and the standard deviations are displayed to the right of the data. (*B*) The diffusion coefficients of LPS-TexasRed in LPS-GUVs correlate with the corresponding LPS content in the membrane. To see this figure in color, go online.
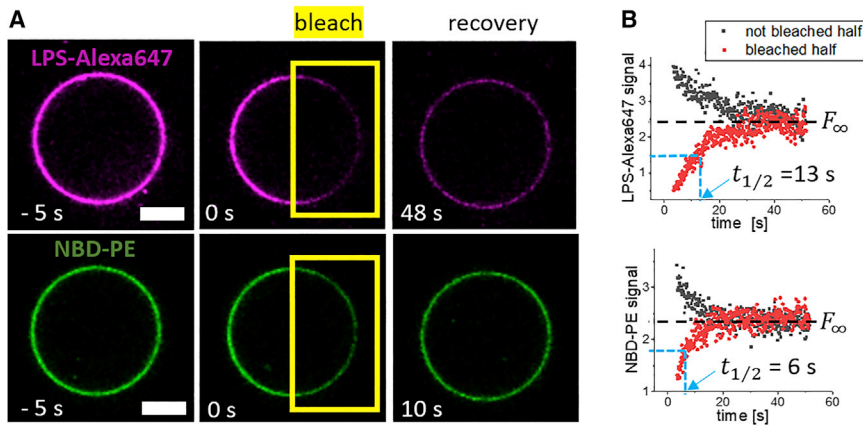
FIGURE 8 Bleaching of the GUV half to assess the ratio of the recovery times of lipids and LPS in the same vesicle. (*A*) Half-GUV FRAP illustrated with images from one vesicle sequentially acquired in two different channels (LPS-Alexa647 in *magenta* and NBD-PE in *green*). The fluorescence on both halves of the GUV is equilibrated after 10 and 48 s for NBD-PE and LPS-Alexa647, respectively. (*B*) The recovery data illustrate the equilibration of the fluorescence signals at both vesicle halves after the bleaching. The halftime of recovery is assessed via Eq. 3. The ratio of the half-recovery time of LPS-Alexa647 to NBD-PE on the same vesicle is 2.33 ± 0.50 (*n* = 6). The scale bar corresponds to 20 μm. To see this figure in color, go online.

by spontaneous curvature resulting from the LPS asymmetric distribution. The vesicles were stable for at least 2 days and retained the LPS molecules in the membrane even after a washing step in a microfluidic chip. The GUVs were employed to determine the diffusion coefficients of LPS (4.3 ± 0.8 μm^2 s^{-1}) and lipids (5.3 ± 1.3 μm^2 s^{-1}) in LPS membranes using conventional FRAP measurements. It was shown that the diffusion coefficient decreased with increasing LPS incorporation. In the context of the heterogeneous LPS content, which is often overlooked, we introduced a calibration standard that allowed the determination of the LPS coverage of individual GUVs. By using this technique, properties of individual LPS GUVs can be directly compared with regard to varying LPS concentrations, which is not possible in bulk compositional studies. We also developed a single-vesicle FRAP assay, in which we directly compare the mobility of lipids and LPS by bleaching and monitoring the recovery in one half of a GUV. This assay allows comparison of diffusivity in the same membrane irrespective of vesicle size and LPS coverage, which vary in different samples. Especially in cases in which conventional spot FRAP cannot be applied because of photobleaching of slow back-diffusing molecules, this variant could serve as an alternative FRAP approach.

Rana et al. showed that in *S.* Typhimurium 30–40 mol % of the OM lipids are composed of LPS (79). However, LPS is present exclusively on the outer leaflet (80) and covers 88% of the bacterial cell surface (81). Since the remaining 12% is mainly covered by proteins and only very small amounts of phospholipids are present (80–83), the actual LPS-lipid ratio at the outer leaflet is likely to be much higher. Although the LPS concentrations in our membrane model were lower compared with the natural compositions of the outer leaflet, the inferred LPS content in the LPS vesicles was in a similar range to the LPS incorporation in symmetrical LPS GUVs by Kubiak et al. (17).

We hypothesize that the limited incorporation of smooth LPS into artificial membranes was caused by its unique molecular properties, especially its tendency to form aggregates. To face the high self-aggregation rate in aqueous solutions, extra steps and considerations were necessary. Several freeze/thaw cycles and ultrasound treatment of the LPS solutions were crucial to break larger LPS aggregates. To further support the assembly at the water-oil interface, an additional emulsification step increased the surface of water-oil interface and reduced diffusion distances. Furthermore, we assume that the dispersed oil droplets interfered with the LPS micelles and caused fusion of micellar structures and emulsion droplets. Centrifugation forces the emulsion droplets back to the continuous interface, relocating the LPS molecules to cluster here.

Despite the limited LPS incorporation, the generated vesicles can serve as a membrane model to study the effects of asymmetrically distributed LPS molecules on membrane properties and their changes at different LPS concentrations. By incorporating additional membrane components, such as OM proteins and bacterial lipids, the LPS-GUVs open a path toward a bottom-up approach of generating more complex membranes in which the effect of antimicrobial agents could be explored.

SUPPORTING MATERIAL

AUTHOR CONTRIBUTIONS

R.D., T.R., and S.B. proposed and supervised the project. R.D., T.R., S.B., and M.S. designed the experiments. M.S. performed the experiments and analyzed the data. S.C. and V.D. provided the analysis of the FCS and sFCS data. S.P. provided the microfluidic chips. R.D., T.R., S.B., V.D., and M.S. wrote the manuscript.

ACKNOWLEDGMENTS

DECLARATION OF INTERESTS

The authors declare no competing interests.

REFERENCES

1. World Health Organization (WHO). Antibiotic Resistance. Fact sheets. https://www.who.int/news-room/fact-sheets/detail/antibiotic-resistance.

2. Nikaido, H. 2003. Molecular basis of bacterial outer membrane permeability revisited. *Microbiol. Mol. Biol. Rev.* 67:593–656.

3. Caroff, M., and D. Karibian. 2003. Structure of bacterial lipopolysaccharides. *Carbohydr. Res.* 338:2431–2447.

4. Raetz, C. R. H., and C. Whitfield. 2002. Lipopolysaccharide endotoxins. *Annu. Rev. Biochem.* 71:635–700.

5. Wilkinson, S. G. 1996. Bacterial lipopolysaccharides—themes and variations. *Prog. Lipid Res.* 35:283–343.

6. Clifton, L. A., M. W. A. Skoda, …, J. H. Lakey. 2015. Effect of divalent cation removal on the structure of gram-negative bacterial outer membrane models. *Langmuir.* 31:404–412.

7. Aurell, C. A., and A. O. Wistrom. 1998. Critical aggregation concentrations of gram-negative bacterial lipopolysaccharides (LPS). *Biochem. Biophys. Res. Commun.* 253:119–123.

8. Dimova, R., and C. Marques. 2019. The Giant Vesicle Book, 1st Edition. CRC Press.

9. Schwille, P., J. Spatz, …, K. Sundmacher. 2018. MaxSynBio: avenues towards creating cells from the bottom up. *Angew. Chem. Int. Ed. Engl.* 57:13382–13392.

10. Guindani, C., L. C. da Silva, …, K. Landfester. 2022. Synthetic cells: from simple bio-inspired modules to sophisticated integrated systems. *Angew. Chem. Int. Ed. Engl.* 61:e202110855.

11. Walde, P., K. Cosentino, …, P. Stano. 2010. Giant vesicles: preparations and applications. *Chembiochem.* 11:848–865.

12. Matosevic, S. 2012. Synthesizing artificial cells from giant unilamellar vesicles: state-of-the art in the development of microfluidic technology. *Bioessays.* 34:992–1001.

13. van Swaay, D., and A. DeMello. 2013. Microfluidic methods for forming liposomes. *Lab Chip.* 13:752–767.

14. Patil, Y. P., and S. Jadhav. 2014. Novel methods for liposome preparation. *Chem. Phys. Lipids.* 177:8–18.

15. Stein, H., S. Spindler, …, V. Sandoghdar. 2017. Production of isolated giant unilamellar vesicles under high salt concentrations. *Front. Physiol.* 8:63.

16. Dimova, R. 2019. Giant vesicles and their use in assays for assessing membrane phase state, curvature, mechanics, and electrical properties. *Annu. Rev. Biophys.* 48:93–119.

17. Kubiak, J., J. Brewer, …, L. A. Bagatolli. 2011. Lipid lateral organization on giant unilamellar vesicles containing lipopolysaccharides. *Biophys. J.* 100:978–986.

18. Dijkstra, J., J. L. Ryan, and F. C. Szoka. 1988. A procedure for the efficient incorporation of wild-type lipopolysaccharide into liposomes for use in immunological studies. *J. Immunol. Methods.* 114:197–205.

19. Paulowski, L., A. Donoghue, T. Gutsmann…, 2020. The beauty of asymmetric membranes: reconstitution of the outer membrane of gram-negative bacteria. *Front. Cell Dev. Biol.* 8:586.

20. Henning, M. F., S. Sanchez, and L. Bakás. 2009. Visualization and analysis of lipopolysaccharide distribution in binary phospholipid bilayers. *Biochem. Biophys. Res. Commun.* 383:22–26.

21. Nair, K. S., N. B. Raj, …, H. Bajaj. 2022. Curved membrane structures induced by native lipids in giant vesicles. *J. Colloid Interface Sci.* 611:397–407.

22. Weinberger, A., F.-C. Tsai, …, C. Marques. 2013. Gel-assisted formation of giant unilamellar vesicles. *Biophys. J.* 105:154–164.

23. Träuble, H., and E. Grell. 1971. Carriers and specificity in membranes. IV. Model vesicles and membranes. The formation of asymmetrical spherical lecithin vesicles. *Neurosci. Res. Program Bull.* 9:373–380.

24. Szoka, F., and D. Papahadjopoulos. 1980. Comparative properties and methods of preparation of lipid vesicles (liposomes). *Annu. Rev. Biophys. Bioeng.* 9:467–508.

25. Pautot, S., B. J. Frisken, and D. A. Weitz. 2003. Production of unilamellar vesicles using an inverted emulsion. *Langmuir.* 19:2870–2879.

26. Noireaux, V., and A. Libchaber. 2004. A vesicle bioreactor as a step toward an artificial cell assembly. *Proc. Natl. Acad. Sci. USA.* 101:17669–17674.

27. Matosevic, S., and B. M. Paegel. 2011. Stepwise synthesis of giant unilamellar vesicles on a microfluidic assembly line. *J. Am. Chem. Soc.* 133:2798–2800.

28. Enoki, T. A., and G. W. Feigenson. 2019. Asymmetric bilayers by hemifusion: method and leaflet behaviors. *Biophys. J.* 117:1037–1050.

29. Enoki, T. A., J. Wu, …, G. W. Feigenson. 2021. Investigation of the domain line tension in asymmetric vesicles prepared via hemifusion. *Biochim. Biophys. Acta. Biomembr.* 1863:183586.

30. Doktorova, M., F. A. Heberle, …, D. Marquardt. 2018. Preparation of asymmetric phospholipid vesicles for use as cell membrane models. *Nat. Protoc.* 13:2086–2101.

31. Chiantia, S., P. Schwille, …, E. London. 2011. Asymmetric GUVs prepared by MβCD-mediated lipid exchange: an FCS study. *Biophys. J.* 100:L1–L3.

32. Scott, H. L., K. B. Kennison, …, J. Katsaras. 2021. Model membrane systems used to study plasma membrane lipid asymmetry. *Symmetry.* 13:1356.

33. Richmond, D. L., E. M. Schmid, …, D. A. Fletcher. 2011. Forming giant vesicles with controlled membrane composition, asymmetry, and contents. *Proc. Natl. Acad. Sci. USA.* 108:9431–9436.

34. Maktabi, S., J. W. Schertzer, and P. R. Chiarot. 2019. Dewetting-induced formation and mechanical properties of synthetic bacterial outer membrane models (GUVs) with controlled inner-leaflet lipid composition. *Soft Matter.* 15:3938–3948.

35. Pautot, S., B. J. Frisken, and D. A. Weitz. 2003. Engineering asymmetric vesicles. *Proc. Natl. Acad. Sci. USA.* 100:10718–10721.

36. Moga, A., N. Yandrapalli, …, T. Robinson. 2019. Optimization of the inverted emulsion method for high-yield production of biomimetic giant unilamellar vesicles. *Chembiochem.* 20:2674–2682.

37. Darveau, R. P., and R. E. Hancock. 1983. Procedure for isolation of bacterial lipopolysaccharides from both smooth and rough Pseudomonas aeruginosa and Salmonella typhimurium strains. *J. Bacteriol.* 155:831–838.

38. Westphal, O., and K. Jann. 1965. Bacterial lipopolysaccharides—extraction with phenol water and further application of the procedure. *Methods Carbohyd. Chem.* 5:83–91.

39. Lee, C.-H., and C.-M. Tsai. 1999. Quantification of bacterial lipopolysaccharides by the purpald assay: measuring formaldehyde generated from 2-keto-3-deoxyoctonate and heptose at the inner core by periodate oxidation. *Anal. Biochem.* 267:161–168.

40. Maia, J., R. A. Carvalho, …, M. H. Gil. 2011. Insight on the periodate oxidation of dextran and its structural vicissitudes. *Polymer.* 52:258–265.

41. Andres, D., C. Hanke, …, R. Seckler. 2010. Tailspike interactions with lipopolysaccharide effect DNA ejection from phage P22 particles in vitro. *J. Biol. Chem.* 285:36768–36775.

42. Miller, S., B. Schuler, and R. Seckler. 1998. Phage P22 tailspike protein: removal of head-binding domain unmasks effects of folding mutations on native-state thermal stability. *Protein Sci.* 7:2223–2232.

43. McIntyre, J. C., and R. G. Sleight. 1991. Fluorescence assay for phospholipid membrane asymmetry. *Biochemistry.* 30:11819–11827.

44. Pramanik, S., J. Steinkühler, …, R. Lipowsky. 2022. Binding of His-tagged fluorophores to lipid bilayers of giant vesicles. *Soft Matter.* 18:6372–6383.

45. Kang, M., C. A. Day, …, E. DiBenedetto. 2012. Simplified equation to extract diffusion coefficients from confocal FRAP data. *Traffic.* 13:1589–1600.

46. Lira, R. B., J. Steinkühler, …, K. A. Riske. 2016. Posing for a picture: vesicle immobilization in agarose gel. *Sci. Rep.* 6:25254.

47. Dunsing, V., T. Irmscher, …, S. Chiantia. 2019. Purely polysaccharide-based biofilm matrix provides size-selective diffusion barriers for nanoparticles and bacteriophages. *Biomacromolecules.* 20:3842–3854.

48. Dunsing, V., and S. Chiantia. 2018. A fluorescence fluctuation spectroscopy assay of protein-protein interactions at cell-cell contacts. *J. Vis. Exp.* 142, e58582.

49. Gendron, P.-O., F. Avaltroni, and K. J. Wilkinson. 2008. Diffusion coefficients of several rhodamine derivatives as determined by pulsed field gradient–nuclear magnetic resonance and fluorescence correlation spectroscopy. *J. Fluoresc.* 18:1093–1101.

50. Dunsing, V., M. Mayer, …, S. Chiantia. 2017. Direct evidence of amyloid precursor–like protein 1 trans interactions in cell–cell adhesion platforms investigated via fluorescence fluctuation spectroscopy. *Mol. Biol. Cell.* 28:3609–3620.

51. Pautot, S. 2002. Self-assembly behavior of lipids at an oil-water interface. Harvard university, ProQuest Dissertation Publishing.

52. Chowdhury, A. U., G. J. Taylor, …, B. Doughty. 2020. Insight into the mechanisms driving the self-assembly of functional interfaces: moving from lipids to charged amphiphilic oligomers. *J. Am. Chem. Soc.* 142:290–299.

53. Hossein, A., and M. Deserno. 2020. Spontaneous curvature, differential stress, and bending modulus of asymmetric lipid membranes. *Biophys. J.* 118:624–642.

54. Bhatia, T., S. Christ, …, R. Lipowsky. 2020. Simple sugars shape giant vesicles into multispheres with many membrane necks. *Soft Matter.* 16:1246–1258.

55. Schneck, E., T. Schubert, …, M. Tanaka. 2010. Quantitative determination of ion distributions in bacterial lipopolysaccharide membranes by grazing-incidence X-ray fluorescence. *Proc. Natl. Acad. Sci. USA.* 107:9147–9151.

56. Ali Doosti, B., W. Pezeshkian, …, T. Lobovkina. 2017. Membrane tubulation in lipid vesicles triggered by the local application of calcium ions. *Langmuir.* 33:11010–11017.

57. Graber, Z. T., Z. Shi, and T. Baumgart. 2017. Cations induce shape remodeling of negatively charged phospholipid membranes. *Phys. Chem. Chem. Phys.* 19:15285–15295.

58. Sinn, C. G., M. Antonietti, and R. Dimova. 2006. Binding of calcium to phosphatidylcholine–phosphatidylserine membranes. *Colloids Surf. A Physicochem. Eng. Asp.* 282–283:410–419.

59. Lira, R. B., F. S. C. Leomil, …, R. Dimova. 2021. To close or to collapse: the role of charges on membrane stability upon pore formation. *Adv. Sci.* 8:2004068.

60. Schneck, E., E. Papp-Szabo, …, M. Tanaka. 2009. Calcium ions induce collapse of charged O-side chains of lipopolysaccharides from Pseudomonas aeruginosa. *J. R. Soc. Interface.* 6:S671–S678.

61. Cray, J. A., J. T. Russell, …, J. E. Hallsworth. 2013. A universal measure of chaotropicity and kosmotropicity. *Environ. Microbiol.* 15:287–296.

62. Nikolov, V., R. Lipowsky, and R. Dimova. 2007. Behavior of giant vesicles with anchored DNA molecules. *Biophys. J.* 92:4356–4368.

63. Dasgupta, R., M. S. Miettinen, …, R. Dimova. 2018. The glycolipid GM1 reshapes asymmetric biomembranes and giant vesicles by curvature generation. *Proc. Natl. Acad. Sci. USA.* 115:5756–5761.

64. Lipowsky, R. 2013. Spontaneous tubulation of membranes and vesicles reveals membrane tension generated by spontaneous curvature. *Faraday Discuss.* 161:305–331, discussion 419-59.

65. Steinkühler, J., P. De Tillieux, …, R. Dimova. 2018. Charged giant unilamellar vesicles prepared by electroformation exhibit nanotubes and transbilayer lipid asymmetry. *Sci. Rep.* 8:11838.

66. Steinkühler, J., P. Fonda, …, R. Dimova. 2021. Superelasticity of plasma and synthetic membranes resulting from coupling of membrane asymmetry, curvature, and lipid sorting. *Adv. Sci.* 8:2102109.

67. Sreekumari, A., and R. Lipowsky. 2018. Lipids with bulky head groups generate large membrane curvatures by small compositional asymmetries. *J. Chem. Phys.* 149:084901.

68. Bassereau, P., R. Jin, …, T. R. Weikl. 2018. The 2018 biomembrane curvature and remodeling roadmap. *J. Phys. D Appl. Phys.* 51:343001.

69. Karimi, M., J. Steinkühler, …, R. Dimova. 2018. Asymmetric ionic conditions generate large membrane curvatures. *Nano Lett.* 18:7816–7821.

70. Dimova, R., and R. Lipowsky. 2017. Giant vesicles exposed to aqueous two-phase systems: membrane wetting, budding processes, and spontaneous tubulation. *Adv. Mater. Interfaces.* 4:1600451.

71. Bhatia, T., J. Agudo-Canalejo, …, R. Lipowsky. 2018. Membrane nanotubes increase the robustness of giant vesicles. *ACS Nano.* 12:4478–4485.

72. Miettinen, M. S., and R. Lipowsky. 2019. Bilayer membranes with frequent flip-flops have tensionless leaflets. *Nano Lett.* 19:5011–5016.

73. Takeuchi, Y., and H. Nikaido. 1981. Persistence of segregated phospholipid domains in phospholipid-lipopolysaccharide mixed bilayers: studies with spin-labeled phospholipids. *Biochemistry.* 20:523–529.

74. Snyder, S., D. Kim, and T. J. McIntosh. 1999. Lipopolysaccharide bilayer structure: effect of chemotype, core mutations, divalent cations, and temperature. *Biochemistry.* 38:10758–10767.

75. Herrmann, M., E. Schneck, …, M. Tanaka. 2015. Bacterial lipopolysaccharides form physically cross-linked, two-dimensional gels in the presence of divalent cations. *Soft Matter.* 11:6037–6044.

76. Paracini, N., E. Schneck, …, S. Micciulla. 2022. Lipopolysaccharides at solid and liquid interfaces: models for biophysical studies of the gram-negative bacterial outer membrane. *Adv. Colloid Interface Sci.* 301:102603.

77. Brandenburg, K., and U. Seydel. 1984. Physical aspects of structure and function of membranes made from lipopolysaccharides and free lipid A. *Biochim. Biophys. Acta Biomembr.* 775:225–238.

78. Naumann, D., C. Schultz, …, H. Labischinski. 1989. New insights into the phase behaviour of a complex anionic amphiphile: architecture and dynamics of bacterial deep rough lipopolysaccharide membranes as seen by FTIR, X-ray, and molecular modelling techniques. *J. Mol. Struct.* 214:213–246.

79. Rana, F. R., C. M. Sultany, and J. Blazyk. 1991. Determination of the lipid composition of Salmonella typhimurium outer membranes by 31P NMR. *J. Microbiol. Methods.* 14:41–51.

80. Funahara, Y., and H. Nikaido. 1980. Asymmetric localization of lipopolysaccharides on the outer membrane of Salmonella typhimurium. *J. Bacteriol.* 141:1463–1465.

81. Smit, J., Y. Kamio, and H. Nikaido. 1975. Outer membrane of Salmonella typhimurium: chemical analysis and freeze-fracture studies with lipopolysaccharide mutants. *J. Bacteriol.* 124:942–958.

82. Kamio, Y., and H. Nikaido. 1976. Outer membrane of Salmonella typhimurium: accessibility of phospholipid head groups to phospholipase C and cyanogen bromide activated dextran in the external medium. *Biochemistry.* 15:2561–2570.

83. Shukla, S. D., C. Green, and J. M. Turner. 1980. Phosphatidylethanolamine distribution and fluidity in outer and inner membranes of the gram-negative bacterium Erwinia carotovora. *Biochem. J.* 188:131–135.